



Synthesis, crystal structure, and nonlinear optical properties of $\text{Bi}_2\text{Cu}_5\text{B}_4\text{O}_{14}$

Shilie Pan^{a,*}, Jared P. Smit^b, Michael R. Marvel^b, Evan S. Stampler^b, Jacob M. Haag^b, Jaewook Baek^c, P. Shiv Halasyamani^c, Kenneth R. Poeppelmeier^b

^a Xinjiang Technical Institute of Physics and Chemistry, Chinese Academy of Sciences, 40-1 South Beijing Road, Urumqi, Xinjiang 830011, China

^b Department of Chemistry, Northwestern University, 2145 Sheridan Road, Evanston, IL 60208-3113, USA

^c Department of Chemistry, University of Houston, 136 Fleming Building, Houston, TX 77204-5003, USA

ARTICLE INFO

Article history:

Received 1 February 2008

Received in revised form

29 April 2008

Accepted 4 May 2008

Available online 14 May 2008

Keyword:

Crystal growth

Crystal structure

Oxide

Nonlinear optical properties

ABSTRACT

$\text{Bi}_2\text{Cu}_5\text{B}_4\text{O}_{14}$ crystallizes in the noncentrosymmetric triclinic space group $P1$ (No. 1) with cell parameters $a = 10.1381(11)\text{Å}$, $b = 9.3917(11)\text{Å}$, $c = 3.4566(4)\text{Å}$, $\alpha = 105.570(2)^\circ$, $\beta = 92.275(2)^\circ$, $\gamma = 107.783(2)^\circ$, $Z = 1$ and $R_1 = 0.0401$ and $wR_2 = 0.0980$. It is a layered structure that is built up from sheets of rectangular CuO_4 and trigonal BO_3 groups. The sheets are connected by infinite chains of edge shared BiO_6 polyhedra that intersect the bc plane at an angle slightly greater than 90° . The second-harmonic generation efficiency of $\text{Bi}_2\text{Cu}_5\text{B}_4\text{O}_{14}$, using 1064 nm radiation, is about one half times that of KH_2PO_4 .

© 2008 Elsevier Inc. All rights reserved.

1. Introduction

Noncentrosymmetric compounds are of interest owing to their symmetry dependent properties such as second-harmonic generation (SHG), electro-optical effect, photorefractive effect, and piezoelectricity [1–9]. Inorganic borates have long been a focus of research for their variety of noncentrosymmetric structure types, transparency to a wide range of wavelengths, high damage threshold, and high optical quality [10–18]. With the development of optical communications and large-scale integrated circuit semiconductors, interest in nonlinear optical materials is high.

The optical properties of borates are dominated by the BO_x units. Among the various anionic groups, planar BO_3 groups with delocalized valence electrons attract attention because they are responsible for the large SHG coefficients of these materials [19]. In the ternary Bi_2O_3 – CuO – B_2O_3 system, $\text{Bi}_2\text{Cu}_5\text{B}_4\text{O}_{14}$ has been reported in the centrosymmetric space group $P-1$ [20], and $\text{Bi}_4\text{CuB}_2\text{O}_{10}$ has been identified by powder X-ray diffraction [21]. The current work, a search for new borate phases in the Bi_2O_3 – CuO – B_2O_3 system, has led to a reinvestigation of $\text{Bi}_2\text{Cu}_5\text{B}_4\text{O}_{14}$ and determined that it is a noncentrosymmetric material with an SHG response one half times that of KH_2PO_4 . The synthesis, crystal structure, thermal analysis, and nonlinear optical properties of $\text{Bi}_2\text{Cu}_5\text{B}_4\text{O}_{14}$ are reported.

2. Experimental section

2.1. Single-crystal growth

Single crystals of $\text{Bi}_2\text{Cu}_5\text{B}_4\text{O}_{14}$ were grown in air. A covered platinum crucible containing a 1:2:2 molar ratio of Bi_2O_3 (99%, Sigma-Aldrich), CuO (99%, Sigma-Aldrich), and H_3BO_3 (99.99%, Alfa-Aesar) was placed into the center of a vertical programmable temperature Molybdenum furnace. The furnace was heated to a temperature of 840°C at a rate of $10^\circ\text{C}/\text{min}$, maintained for 24 h, cooled to 600°C at a rate of $0.1^\circ\text{C}/\text{min}$, and finally cooled to room temperature at a rate of $10^\circ\text{C}/\text{min}$. Green needle crystals were separated from the flux for the structure determination.

2.2. Single crystal X-ray diffraction

The crystal structure of $\text{Bi}_2\text{Cu}_5\text{B}_4\text{O}_{14}$ was determined by single-crystal X-ray diffraction on a Bruker SMART–1000 CCD diffractometer using monochromatic $\text{MoK}\alpha$ radiation ($\lambda = 0.71073\text{Å}$) and integrated with the SAINT–Plus program [22].

All calculations were performed with programs from the SHELXTL crystallographic software package [23]. The structure was solved by direct methods. A face-indexed absorption correction was performed using the XPREP program, followed by the SADABS program [24]; equivalent reflections were then averaged. Final least-squares refinement is on F_0^2 with data having $F_0^2 \geq 2\sigma(F_0^2)$. Crystal data and structure refinement information are summarized in Table 1 with additional details found in the

* Corresponding author. Fax: +86 991 3838957.

E-mail address: slpan@ms.xjbc.ac.cn (S. Pan).

Table 1
Crystal data and structure refinement for Bi₂Cu₅B₄O₁₄

Empirical formula	Bi ₂ Cu ₅ B ₄ O ₁₄
Temperature	153(2) K
Wavelength	0.71073 Å
Formula weight	1002.90
Crystal system	Triclinic
Space group	P1
Unit cell dimensions	$a = 10.1381(11)$ Å, $\alpha = 105.570(2)^\circ$ $b = 9.3917(11)$ Å, $\beta = 97.275(2)^\circ$ $c = 3.4566(4)$ Å, $\gamma = 104.783(2)^\circ$
Volume	293.98(6) Å ³
Z	1
Density (calculated)	5.665 g/cm ³
Absorption coefficient	38.772 mm ⁻¹
F(000)	443
Crystal size	0.01 × 0.02 × 0.14 mm ³
Theta range for data collection	2.17–28.62°
Index ranges	−13 ≤ h ≤ 13, −12 ≤ k ≤ 12, −4 ≤ l ≤ 4
Reflections collected	2773
Independent reflections	2395 [R(int) = 0.0455]
Completeness to theta = 25	91.5%
Flack parameter	0.06(8)
Max. and min. transmission	0.70598 and 0.12841
Refinement method	Full-matrix least squares on F ²
Data/restraints/parameters	2395/3/136
Goodness-of-fit on F ²	1.009
Final R indices [I > 2σ(I)] ^a	R ₁ = 0.0401, wR ₂ = 0.0980
R indices (all data) ^a	R ₁ = 0.0451, wR ₂ = 0.1010
Largest diff. peak and hole	2.655 and −3.035 e Å ⁻³

$$^a R_1 = \frac{\sum ||F_o| - F_c||}{\sum |F_o|} \text{ and } wR_2 = \left[\frac{\sum w(F_o^2 - F_c^2)^2}{\sum wF_o^4} \right]^{1/2} \text{ for } F_o^2 > 2\sigma(F_o^2).$$

supporting information. Final atomic coordinates and equivalent isotropic displacement parameters are listed in Table 2. Selected interatomic distances and angles are given in Table S1 in the supporting information.

2.3. Solid-state synthesis

Polycrystalline powder samples were synthesized for infrared spectroscopy, differential thermal analysis (DTA), and SHG measurements. Stoichiometric mixtures of Bi₂O₃ (99%, Sigma-Aldrich), CuO (99%, Sigma-Aldrich), and H₃BO₃ (99.99%, Alfa-Aesar) were packed into a platinum crucible and heated at 500 °C for several hours in air to eliminate the water. The reaction mixture was then elevated to a temperature of 710 °C and held for 72 h with intermittent grinding, and cooled to room temperature at a rate of 10 °C/min.

2.4. Powder X-ray diffraction

X-ray powder diffraction analysis of Bi₂Cu₅B₄O₁₄ was performed at room temperature in the angular range of 10° ≤ 2θ ≤ 70° with a scan step width of 0.02° and a fixed counting time of 1 s/step using an automated Rigaku X-ray diffractometer equipped with a diffracted-beam monochromator set for CuKα (λ = 1.5418 Å) radiation. The experimental powder X-ray diffraction pattern of Bi₂Cu₅B₄O₁₄ is in agreement with the calculated data based on the single-crystal data (Figures S1 and S2 in the supporting information).

2.5. Infrared spectroscopy

The infrared spectrum was measured to specify and compare the coordination of boron. The mid-infrared spectrum was obtained at room temperature via a Bio-Rad FTS-60 FTIR spectrometer. The polycrystalline sample was mixed thoroughly with dried KBr (5 mg of the sample, 500 mg of KBr) and pressed into a

Table 2
Atomic coordinates (× 10⁴) and equivalent isotropic displacement parameters (Å² × 10³) for Bi₂Cu₅B₄O₁₄

Atom	wyckoff position	x	y	z	U _{eq}
Bi(1)	1a	8193(1)	653(1)	15939(1)	5(1)
Bi(2)	1a	1692(1)	−2231(1)	3303(1)	6(1)
Cu(1)	1a	9945(8)	4223(10)	14630(20)	5(1)
Cu(2)	1a	3430(6)	−4039(7)	6809(18)	6(1)
Cu(3)	1a	6470(6)	2456(7)	12452(18)	5(1)
Cu(4)	1a	4946(8)	−779(9)	9660(20)	5(1)
Cu(5)	1a	4952(8)	4214(11)	9630(30)	7(1)
B(1)	1a	3330(30)	1300(40)	10610(90)	0(6)
B(2)	1a	1870(30)	2930(30)	8380(90)	2(6)
B(3)	1a	8060(40)	5690(40)	10840(110)	13(8)
B(4)	1a	6660(30)	−2870(40)	8930(100)	4(7)
O(1)	1a	6100(20)	760(30)	14890(70)	3(5)
O(2)	1a	8270(20)	2230(30)	12160(70)	4(5)
O(3)	1a	4530(20)	2530(30)	11980(70)	5(5)
O(4)	1a	6860(30)	4290(30)	10620(80)	10(5)
O(5)	1a	3730(20)	−2400(30)	4330(70)	3(5)
O(6)	1a	1580(30)	−3820(20)	7060(70)	6(5)
O(7)	1a	3060(30)	4140(30)	8630(70)	8(5)
O(8)	1a	3180(30)	−260(30)	10140(70)	5(5)
O(9)	1a	6690(30)	−1340(30)	9160(80)	11(5)
O(10)	1a	2030(20)	1580(30)	9270(70)	9(5)
O(11)	1a	550(20)	3000(30)	7820(60)	5(5)
O(12)	1a	7880(20)	6940(20)	10280(70)	4(4)
O(13)	1a	5330(20)	−4070(30)	7370(70)	5(5)
O(14)	1a	−650(30)	−4500(30)	1470(70)	11(5)

U_{eq} is defined as one-third of the trace of the orthogonalized U_{ij} tensor.

pellet. The spectrum was collected in a range from 400 to 4000 cm⁻¹ with a resolution of 1 cm⁻¹.

2.6. Differential thermal analysis

DTA was performed under static air on a TA Instruments DSC 2910 thermal analyzer. The powder sample and reference (Al₂O₃) were enclosed in Pt crucibles, heated from room temperature to 910 °C, and then cooled to room temperature at a rate of 10 °C/min. A large difference in the heating and cooling curves suggested that Bi₂Cu₅B₄O₁₄ melts incongruently (Figure S3 in the supporting information). To further verify that Bi₂Cu₅B₄O₁₄ melts incongruently, 0.6 g of Bi₂Cu₅B₄O₁₄ polycrystalline powder was heated to 910 °C, and quickly cooled to room temperature. Analysis of the powder X-ray diffraction pattern of the recovered solid in Figure S4 in the supporting information revealed that the diffraction pattern is different from that of the initial Bi₂Cu₅B₄O₁₄ powder, which further suggests that Bi₂Cu₅B₄O₁₄ is an incongruently melting compound. Based on the above X-ray diffraction pattern collected on a sample that has been melted and cooled, the peritectic reaction should be followed by another peak corresponding to complete melting in the heating curve (Figure S3 in the supporting information). This peak is not observed on the heating curve, but may not be visible owing to low intensity. In addition, there is no exothermic peak in the cooling curve (Figure S3 in the supporting information), which could be due to the fast cooling rate of 10 °C/min and the high viscosity for borate melts in general.

2.7. SHG measurement

Powder SHG measurements were carried out on Bi₂Cu₅B₄O₁₄ by means of the Kurtz–Perry method [25]. About 80 mg of polycrystalline powder sample was pressed into a pellet which was then irradiated with a pulsed infrared beam (100 ns, 15 mJ, 10 Hz) produced by a Q-switched Nd:YAG laser of wavelength

1064 nm. A 532 nm filter was used to absorb the fundamental and pass the visible light onto a photomultiplier. A combination of a half-wave achromatic retarder and a polarizer was used to control the intensity of the incident power, which was measured with an identical photomultiplier connected to the same high voltage source. This procedure was then repeated using a standard nonlinear optical material, in this case microcrystalline KH_2PO_4 (KDP), and the ratio of the second-harmonic intensity output was calculated. Since the SHG efficiency of powders has been shown to depend strongly on particle size [25,26], polycrystalline $\text{Bi}_2\text{Cu}_5\text{B}_4\text{O}_{14}$ was ground and sieved (Newark Wire Cloth Company) into distinct particle size ranges, <20, 20–38, 38–53, 53–75, 75–90, 90–105, 105–150, and 150–180 μm . KDP samples were ground and sieved into the same particle size ranges for comparison.

3. Results and discussion

3.1. Crystal structure

$\text{Bi}_2\text{Cu}_5\text{B}_4\text{O}_{14}$ crystallizes in the noncentrosymmetric triclinic space group $P1$. Two unique bismuth atoms, five unique copper atoms, four unique boron atoms, and 14 unique oxygen atoms are in the asymmetric unit. The extended framework is built up from zigzag sheets that consist of rectangular planar CuO_4 and trigonal planar BO_3 groups, shown in Fig. 1. The sheets are connected by infinite chains of edge shared BiO_6 polyhedra that intersect the sheets at an angle slightly greater than 90° , shown in Fig. 2. Cu_3O_8 trimers of edge shared CuO_4 polyhedra, where the three copper atoms are in the same plane, are bordered on each side by BiO_6 polyhedra. The central copper atom of the trimer shares edges with two separate pyroborate groups on each side, forming $\text{CuB}_4\text{O}_{10}$ units similar to those observed in $\text{Li}_6\text{CuB}_4\text{O}_{10}$ [8] (Fig. 1).

The Bi^{3+} cations occupy two distinct sites. The coordination polyhedron of Bi^{3+} cations is asymmetric with three short bonds (2.12(2)–2.24(2) Å) and three longer ones (2.51(3)–2.62(3) Å) (Table S1). Such irregular coordination is common for bismuth

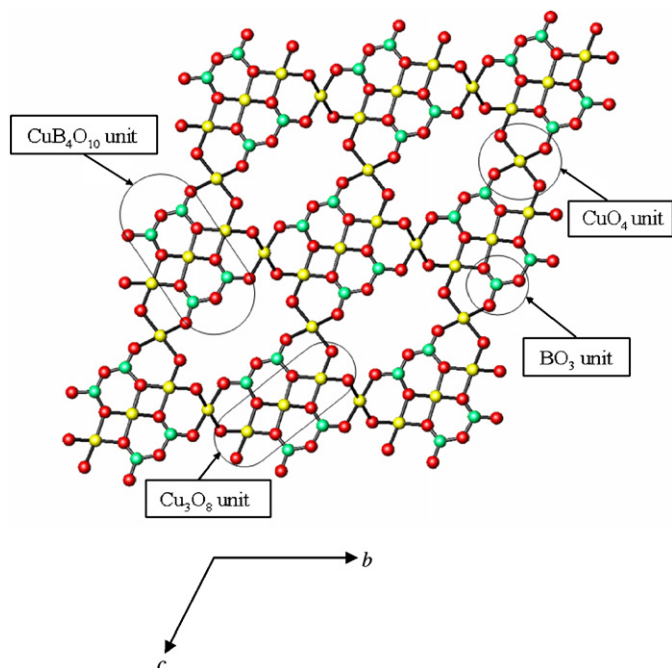


Fig. 1. The two-dimensional layer of interconnected rectangular planar CuO_4 and trigonal planar BO_3 groups in $\text{Bi}_2\text{Cu}_5\text{B}_4\text{O}_{14}$. The yellow spheres are Cu; the green spheres are B; and the red spheres are O atoms (for interpretation of color see the figures in the online version of the paper).

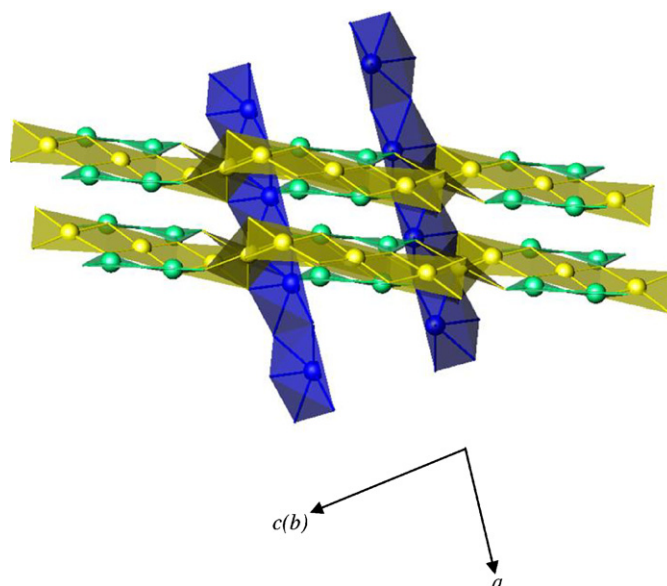


Fig. 2. Infinite chains of edge shared BiO_6 polyhedra intersect the zigzag sheets of interconnected rectangular planar CuO_4 and trigonal planar BO_3 groups. The Bi atoms and BiO_6 polyhedra are blue, the Cu atoms and CuO_4 polyhedra are yellow; and the B atoms and BO_3 polyhedra are green (for interpretation of color see the figures in the online version of the paper).

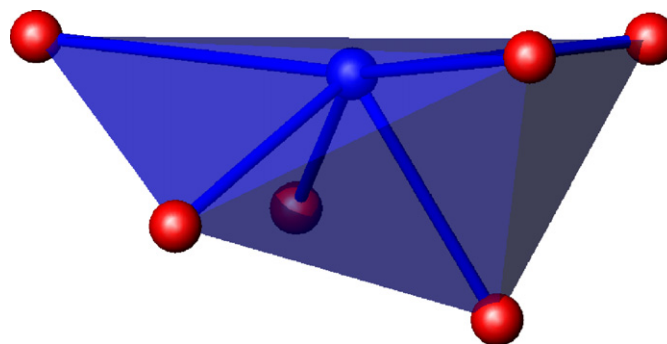


Fig. 3. The coordination polyhedron of Bi^{3+} ion is shown. The blue sphere is Bi, and the red spheres are O atoms (for interpretation of color see the figures in the online version of the paper).

borates [27,28] (Fig. 3) owing in part to the electron lone pair on the Bi^{3+} cation. For the CuO_4 groups, the average Cu–O distance is similar to the Cu–O bond lengths observed in other copper borates such as $\text{Pb}_2\text{CuB}_2\text{O}_6$ and CuB_2O_4 [29,30]. The BO_3 polyhedra are distorted from perfect trigonal planar geometry, as shown by the B–O distances and O–B–O angles listed in Table S1. However, it remains planar (the sum of the O–B–O angles are 360, as seen in Table S1) and the average B–O distances compare to similar interactions observed in a variety of other borates [31–33]. The oxygen coordination varies from two coordinate (O(12) and O(14)) to three coordinate (O(1), O(2), O(3), O(6), O(8), O(10), O(11), and O(13)) to four coordinate (O(4), O(5), O(7), and O(9)) (Table 3). The bond valence sums of each atom in $\text{Bi}_2\text{Cu}_5\text{B}_4\text{O}_{14}$ were calculated [34,35] and are listed in Table 3.

3.2. Vibrational spectroscopic characterization

To further investigate the coordination environment of boron, the infrared spectrum was measured at room temperature and is shown in Figure S5 in the supporting information. Absorptions were assigned from literature precedents [36–38]. The infrared absorption region between about 1100 and 1400 cm^{-1} reveals two

Table 3
Bond valence analysis of the $\text{Bi}_2\text{Cu}_5\text{B}_4\text{O}_{14}$ ^{a,b}

Atom	Bi(1)	Bi(2)	Cu(1)	Cu(2)	Cu(3)	Cu(4)	Cu(5)	B(1)	B(2)	B(3)	B(4)
O(1)		0.857			0.494		0.478				
O(2)	0.955		0.512		0.413						
O(3)						0.581	0.494		0.725		
O(4)		0.330			0.398			0.925			
O(5)		0.240					0.502				
O(6)		0.700	0.473								
O(7)		0.663									1.148
O(8)	0.725		0.494		0.550						
O(9)	0.687		0.494	0.451							
O(10)	0.297			0.440				1.117			
O(11)	0.304			0.409						0.976	
O(12)	0.255										
O(13)		0.287	0.452								0.950
O(14)			0.521		0.491		0.900				
Σ cations	3.223	3.077	2.021	1.816	1.714	2.143	1.937	2.912	2.959	2.920	2.928

^a Bond valences calculated with the program Bond Valence Calculator Version 2.00, Hormillosa, C., Healy, S., Stephen, T. McMaster University (1993).

^b Valence sums calculated with the formula: $S_i = \exp[(R_0 - R_i)/B]$, where S_i : valence of bond "i" and $B = 0.37$.

strong absorption bands (1210 and 1300 cm^{-1}) owing to the B–O asymmetric stretching mode of the trigonal BO_3 groups, while the bands at about 682 cm^{-1} should be attributed to the B–O out-of-plane bending, which confirms the existence of the BO_3 groups.

3.3. Nonlinear optical properties

A preliminary SHG efficiency measurement of $\text{Bi}_2\text{Cu}_5\text{B}_4\text{O}_{14}$ has been carried out by the Kurtz–Perry method using polycrystalline samples at room temperature [25]. The investigation probes properties associated with the determined symmetry group, in particular, the lack of an inversion center. The intensity of the green light (frequency-doubled output: $\lambda = 532\text{ nm}$) produced by the $\text{Bi}_2\text{Cu}_5\text{B}_4\text{O}_{14}$ powder is about one half times that of KDP powder, indicating that $\text{Bi}_2\text{Cu}_5\text{B}_4\text{O}_{14}$ has one half times the SHG efficiency of KDP. $\text{Bi}_2\text{Cu}_5\text{B}_4\text{O}_{14}$ was found to be nonphase-matchable (Figure S6 in the supporting information). That is, as the particle size of $\text{Bi}_2\text{Cu}_5\text{B}_4\text{O}_{14}$ becomes significantly larger than the coherence length of the material, the SHG intensity decreases rapidly [25,26].

A previous structure characterization of $\text{Bi}_2\text{Cu}_5\text{B}_4\text{O}_{14}$ has determined that it crystallizes in the centrosymmetric space group $P-1$ [20], although only the unit cell parameters were given. The SHG signal suggests, however, that $\text{Bi}_2\text{Cu}_5\text{B}_4\text{O}_{14}$ lacks a center of symmetry, and therefore $P1$ is the correct space group, which is consistent with our crystal structure results. During the process of solving the crystal structure of $\text{Bi}_2\text{Cu}_5\text{B}_4\text{O}_{14}$, after the Shelxtl program was used, the program only gave two optional space groups ($P-1$ and $P1$). The centrosymmetric space group $P-1$ was first tried, but the final residual indices ($R1$) for all data is very high (0.1128) after its crystal structure was solved. Then the noncentrosymmetric space group $P1$ was tried, the final residual indices ($R1$) for all data is reasonable (0.0451) after the crystal structure was solved. Although the zigzag sheet (Fig. 1) appears to have a center of symmetry, all of the Cu–O bonds in the CuO_4 polyhedra are different lengths, and each BO_3 polyhedron contains three different B–O bond lengths with various distortions. Furthermore, none of the different BO_3 groups lie within the same plane. When these separate BO_3 groups fall out of plane,

the SHG response is thought to decrease because large NLO effects occur when anionic groups with conjugated π -electron systems such as BO_3 are distributed within the same plane. However, because the different BO_3 groups are nonplanar, $\text{Bi}_2\text{Cu}_5\text{B}_4\text{O}_{14}$ adopts a noncentrosymmetric structure, and ultimately the separate nonplanar BO_3 groups are responsible for the SHG response.

As mentioned, the Bi^{3+} cations are in asymmetric coordination environments owing to their nonbonded electron pair. The net direction of the lone pair polarizations can contribute to the SHG response [3,39]. As depicted in the Fig. 2, the lone pairs on neighboring Bi^{3+} cations are directed towards each other which limits their total NLO contribution.

4. Conclusions

$\text{Bi}_2\text{Cu}_5\text{B}_4\text{O}_{14}$ has been synthesized and its structure has been determined by single crystal X-ray diffraction. It is a layered structure and is built up from zigzag sheets of rectangular planar CuO_4 and triangular planar BO_3 groups that are joined by infinite chains of edge shared BiO_6 polyhedra. $\text{Bi}_2\text{Cu}_5\text{B}_4\text{O}_{14}$ lacks a center of symmetry, and exhibits distinct nonlinear optical properties which are about one half times those of KDP powder.

Auxiliary Material: Further details of the crystal structure investigation may be obtained from the Fachinformationzentrum Karlsruhe, D-76344 Eggenstein-Leopoldshafen, Germany (Fax: +49 7247 808 666; E-mail: crysdata@fiz-karlsruhe.de) on quoting depository number CSD418807.

Supporting information available

An X-ray crystallographic file in CIF format including crystallographic details; calculated and observed X-ray diffraction pattern data; differential thermal analysis plot, the powder X-ray diffraction pattern of the $\text{Bi}_2\text{Cu}_5\text{B}_4\text{O}_{14}$ sample melted and cooled, IR spectrum, phase-matching, i.e., particle size vs SHG intensity data and selected bond lengths (Å) and angles (degrees) for $\text{Bi}_2\text{Cu}_5\text{B}_4\text{O}_{14}$.

Acknowledgments

The authors thank Charlotte L. Stern for assistance with crystallographic measurements. The authors gratefully acknowledge the financial support from the National Science Foundation (Solid State Chemistry Award nos. DMR-0312136 and DMR-0604454), and the Department of Energy, BES-Chemical Sciences, Geosciences, and Biosciences Division under Grant no. DE-FG0203ER15457, the use of the Central Facilities supported by the MRSEC program of the National Science Foundation (DMR-0520513) at the Materials Research Center of Northwestern University and the West Light Foundation of the Chinese Academy of Sciences. JB and PSH thank the Welch Foundation and the NSF (DMR 0652150) for support.

Appendix A. Supplementary data

Supplementary data associated with this article can be found in the online version at doi:10.1016/j.jssc.2008.05.008.

References

- [1] D.J. Williams, *Angew. Chem. Int. Ed. Engl.* 23 (1984) 690–703.
- [2] J. Nye, *Physical Properties of Crystals*, Oxford University Press, Oxford, 1957.
- [3] P.S. Halasyamani, K.R. Poeppelmeier, *Chem. Mater.* 10 (1998) 2753–2769.

- [4] P.A. Maggard, C.L. Stern, K.R. Poeppelmeier, *J. Am. Chem. Soc.* 123 (2001) 7742–7743.
- [5] F. Jona, G. Shirane, *Ferroelectric Crystals*, Pergamon Press, Oxford, 1962.
- [6] W.E. Moerner, S.M. Silence, *Chem. Rev.* 94 (1994) 127–155.
- [7] P. Becker, *Adv. Mater.* 10 (1998) 979–992.
- [8] S. Pan, J.P. Smit, B. Watkins, M.R. Marvel, C.L. Stern, K.R. Poeppelmeier, *J. Am. Chem. Soc.* 128 (2006) 11631–11634.
- [9] K.M. Ok, E.O. Chi, P.S. Halasyamani, *Chem. Soc. Rev.* 35 (2006) 710–717.
- [10] C. Chen, B. Wu, A. Jiang, G. You, *Sci. Sin. B* 28 (1985) 235–243.
- [11] C. Chen, Y. Wu, A. Jiang, G. You, R. Li, S. Lin, *J. Opt. Soc. Am. B* 6 (1989) 616–621.
- [12] Y. Wu, T. Sasaki, S. Nakai, A. Yokotani, H. Tang, C. Chen, *Appl. Phys. Lett.* 74 (1993) 7014–7015.
- [13] G. Aka, A. Kahn-Harari, D. Vivien, Z.-M. Benitez, F. Salin, J. Godard, *Eur. J. Solid State Inorg. Chem.* 33 (1996) 727–736.
- [14] C. Chen, Y. Wang, B. Wu, K. Wu, W. Zeng, L. Yu, *Nature* 373 (1995) 322–323.
- [15] Z. Hu, T. Higashiyama, M. Yoshimura, Y. Mori, T. Sasaki, *J. Cryst. Growth* 212 (2000) 368–371.
- [16] T. Sasaki, Y. Mori, M. Yoshimura, Y.K. Yap, T. Kamimura, *Mater. Sci. Eng. R* 30 (2000) 1–54.
- [17] Y. Wu, J. Liu, P. Fu, J. Wang, H. Zhou, G. Wang, C. Chen, *Chem. Mater.* 13 (2001) 753–755.
- [18] S. Pan, Y. Wu, P. Fu, G. Zhang, Z. Li, C. Du, C. Chen, *Chem. Mater.* 15 (2003) 2218–2221.
- [19] C. Chen, G. Liu, *Annu. Rev. Mater. Sci.* 16 (1986) 203–243.
- [20] G.A. Petrakovskii, K.A. Sablina, A.I. Pankrats, D.A. Velikanov, A.D. Balaev, O.A. Bayukov, V.I. Tugarinov, A.M. Vorotynov, A.D. Vasil'ev, G.V. Romanenko, Yu.G. Shvedenkov, *Phys. Solid State* 44 (2002) 1339–1344.
- [21] M.I. Zargarova, N.M. Mustafaev, N.S. Shuster, *Inorg. Mater.* 32 (1996) 65–70.
- [22] SAINT—Plus, version 6.02A, Bruker Analytical X-ray Instruments, Inc., Madison, WI, 2000.
- [23] G.M. Sheldrick, SHELXTL, Version 6.14, Bruker Analytical X-ray Instruments, Inc., Madison, WI, 2003.
- [24] Bruker SMART Version 5.054, and SADABS version 2.05, Bruker Analytical X-ray Systems, Inc., Madison, WI, 2003.
- [25] S.Q. Kurtz, T.T. Perry, *J. Appl. Phys.* 39 (1968) 3798–3813.
- [26] J.P. Dougherty, S.K. Kurtz, *J. Appl. Crystallogr.* 9 (1976) 145–158.
- [27] L. Li, G. Li, Y. Wang, F. Liao, J. Lin, *Chem. Mater.* 17 (2005) 4174–4180.
- [28] J. Barbier, N. Penin, L.M. Cranswick, *Chem. Mater.* 17 (2005) 3130–3136.
- [29] S. Pan, J.P. Smit, M.R. Marvel, C.L. Stern, B. Watkins, K.R. Poeppelmeier, *Mater. Res. Bull.* 41 (2006) 916–924.
- [30] M. Martinez-Ripoll, S. Martinez-Carrera, S. Garcia-Blanco, *Acta. Crystallogr.* 27B (1971) 677–681.
- [31] D.A. Keszler, H. Sun, *Acta. Crystallogr.* 44C (1988) 1505–1507.
- [32] J. Barbier, N. Penin, A. Denoyer, L.M.D. Cranswick, *Solid State Sci.* 7 (2005) 1055–1061.
- [33] L. Li, Y. Wang, F. Liao, J. Lin, *Inorg. Chem.* 44 (2005) 8243–8248.
- [34] I.D. Brown, D. Altermatt, *Acta. Crystallogr.* 41B (1985) 244–247.
- [35] N.E. Brese, M. O'Keefe, *Acta. Crystallogr.* 47B (1991) 192–197.
- [36] A. Rulmont, M. Almou, *Spectrochim. Acta.* 45A (1989) 603–610.
- [37] S.D. Ross, in: V.C. Farmer (Ed.), *The Infrared Spectra of Minerals*, Adlard, Dorking, Surrey, 1974, p. 205.
- [38] L. Wu, X.L. Chen, Y.P. Xu, Y.P. Sun, *Inorg. Chem.* 45 (2006) 3042–3047.
- [39] Z. Lin, Z. Wang, C. Chen, M. Lee, *J. Appl. Phys.* 90 (2001) 5585–5590.